

# Photometric Solutions for Detached Eclipsing Binaries: selection of ideal distance indicators in the SMC

J. S. B. Wyithe<sup>1,2</sup>, R. E. Wilson<sup>3</sup>

## ABSTRACT

Detached eclipsing binary stars provide a robust one-step distance determination to nearby galaxies. As a by-product of Galactic microlensing searches, catalogs of thousands of variable stars including eclipsing binaries have been produced by the OGLE, MACHO and EROS collaborations. We present photometric solutions for detached eclipsing binaries in the Small Magellanic Cloud (SMC) discovered by the OGLE collaboration. The solutions were obtained with an automated version of the Wilson-Devinney program. By fitting mock catalogs of eclipsing binaries we find that the normalized stellar radii (particularly their sum) and the surface brightness ratio are accurately described by the fitted parameters and estimated standard errors, despite various systematic uncertainties. In many cases these parameters are well constrained. In addition we find that systems exhibiting complete eclipses can be reliably identified where the fractional standard errors in the radii are small. We present two quantitatively selected sub-samples of eclipsing binaries that will be excellent distance indicators. These can be used both for computation of the distance to the SMC and to probe its structure. One particularly interesting binary has a very well determined solution, exhibits complete eclipses, and is comprised of well detached G-type, class *II* giants.

*Subject headings:* stars: eclipsing binaries - distance scale

## 1. Introduction

The goal of the Hubble Space Telescope (HST) Key project on the extragalactic distance scale is to measure the redshift - distance relation from Cepheid variables (e.g. Freedman

---

<sup>1</sup>Princeton University Observatory, Peyton Hall, Princeton, NJ 08544, USA

<sup>2</sup>School of Physics, The University of Melbourne, Parkville, Vic, 3052, Australia

<sup>3</sup>Astronomy Department, University of Florida, Gainesville, FL 32611

et al. 2001). However, the distance modulus for the Large Magellanic Cloud (LMC) that normalizes the HST Cepheid distances is a matter of some debate. Because the extrema of published results formally differ at the  $3\sigma$  level (Gibson 1999), it is clear that significant and unappreciated systematic uncertainties exist in some or all of the methods. It has been argued (Paczynski 1997, 2000) that with current technology, detached eclipsing binaries provide the most direct and accurate distance to the Magellanic Clouds (see Paczynski 1997 for a simple outline of the method, and Kruszewski & Semeniuk 1999 for an historical outlook). Two examples (for the LMC) are already in the literature (Guinan et al. 1998; Fitzpatrick et al. 2001), demonstrating the potential of the technique. Furthermore, a consistency check on the eclipsing binary method was presented by Semeniuk (2000), who compared detached eclipsing binary parallaxes by Lacy (1979) with Hipparcos parallaxes and found good agreement. The attributes of the most promising eclipsing binary systems for distance determination were discussed by Paczynski (1997). The two stars should be similar, in size and effective temperature, and have radii much smaller than the stellar separation. In addition, the inclination should be high to facilitate deep eclipses. Furthermore, the most reliable distances will come from objects that are subject to very small amounts of interstellar reddening. Systems where the stars are completely eclipsed are particularly important because they can provide robust measurements of the ratio of radii. In this paper we have restricted our attention to detached eclipsing binaries. However we note that semi-detached and over-contact systems often have photometric solutions that are better constrained, and will also be useful for distance determination. We define over-contact to mean that both stars exceed their critical lobes (*viz.* Wilson, 2001).

With high quality spectroscopic and photometric observations, standard eclipsing binary light curve fitting routines provide accurate masses, sizes and surface brightness ratios for the components of a double lined eclipsing binary. Indeed, eclipsing binaries have been a primary source of fundamental stellar data (e.g. Andersen 1991). The distance to an eclipsing binary follows from the dimensions thus determined plus the absolute surface brightnesses, which are inferred from the spectral types, either through model atmospheres or an empirical relation. Empirical studies of the surface brightness - color relation are based on the determination of stellar radii by interferometry (e.g. Di Benedetto 1998; van Belle et al. 1999). Eclipsing binaries with independently measured distances can also be used to calibrate the relation. Kruszewski & Semeniuk (1999) published a list of nearby EA-type eclipsing binaries with measured Hipparcos parallaxes for this purpose, and argued that it was the superior method.

In recent years the massive photometric monitoring programs (primarily for microlensing) directed toward the Magellanic clouds have discovered large numbers of variable stars including eclipsing binaries (e.g. Grison et al. 1995; Alcock et al. 1997; Udalski et al. 1998). These catalogs motivate systematic searches for rare, close to ideal systems. Alcock

et al. (1997) presented photometric fits to 611 eclipsing binaries in the LMC based on the Nelson-Davis-Etzel model (Etzel 1981; Popper & Etzel 1981). Here we use the catalog of eclipsing binaries produced for the Small Magellanic Cloud (SMC) by the OGLE collaboration (Udalski et al. 1998, see that paper for details of the catalog selection), which has dense photometric I-band light curves for 1459 eclipsing binaries. The light curves are publically available from <http://bulge.princeton.edu/~ogle/>. We describe an automated light curve fitting procedure and carry out solutions for detached OGLE SMC binaries. Our primary aim is to select detached systems that are most suitable for distance determination. Semi-detached and over-contact eclipsing binaries in the SMC will be discussed in a subsequent paper. This work is a first step toward an eclipsing binary fitting pipeline with a realistic and physically motivated model.

Sec. 2 discusses our automated fitting scheme. In Sec. 3 we display light curve fits to simulated eclipsing binary catalogs in order to gauge reliability. Sec. 4 discusses two lists of the best detached candidates for distance determination selected from the OGLE catalog. These lists are compared with the subjective list compiled by Udalski et al. (1998). We also list solutions for the 57 candidate OGLE systems.

## 2. The Fitting Scheme

We use a public program (Wilson & Devinney 1971; Wilson 1979, 1990, 1998) that, in its distributed form, requires user interaction at every iteration. This lack of automation is a way to force users to examine the progress of a solution. However, while detailed fits to individual eclipsing binaries should be carried out interactively, the large number of systems (1459) investigated here makes continual interaction impractical. We have therefore constructed an automated version of the Differential Corrections program.

### 2.1. the automated fitting scheme

The FORTRAN program *lc.f* produces a light curve from input parameters, while *dc.f* improves a solution and estimates parameter uncertainties using the method of differential corrections. Our implementation of automation is via a shell script written in PERL that executes *dc*, as well as a number of auxiliary programs that create and update the input for *dc*, test for solution convergence, and create output using *lc*. While other methods might be faster, this approach allows *dc.f* to remain virtually unaltered. Future additions to *dc* can therefore be easily incorporated. The several morphological types of binary (*i.e.* detached,

semi-detached, etc.) are handled by corresponding operational modes of *lc* and *dc*. The PERL script attempts to fit each object in mode 2, which is for detached systems. Initial parameter guesses are taken from a large pre-calculated library of eclipsing binary light curves. This is efficient, given the large number of objects. A best fit is first found for each library curve by adjusting the initial epoch,  $T_0$ . We assume the period determined by Udalski et al. (1998). The library curve with the closest fit is then used as the initial guess (with luminosities scaled appropriately). We feel this to be a better approach than attempting to estimate the parameters from eclipse widths, positions, and depths, due to the relatively noisy data.

The method of multiple subsets (Wilson & Biermann 1976) and the Marquardt algorithm (Marquardt 1963; Levenberg 1944) with  $\lambda = 10^{-5}$  were used to improve convergence. Our implementation proceeds from the initial guess via sequential iterations, each consisting of an execution of *dc* for each of the 3 parameter subsets (parameters are updated after each subset run), followed by an execution with the whole parameter set (for the estimation of standard errors). Convergence is defined to have been achieved if parameter adjustments from each of the individual subset runs are smaller than 0.2 times the standard errors (calculated from running *dc* on the full parameter set). Two groups of subsets are defined. If the solution fails to converge or moves to an unphysical region of parameter space with the first group, the iteration is terminated and convergence is sought from the initial guess for the second group. We demand that convergence be achieved only for the parameters corresponding to the surface potentials ( $\Omega$ ), effective temperature ( $T$ ), luminosity ( $L$ ), and inclination ( $i$ ). We found that eccentricity ( $e$ ) and initial epoch were often much slower to converge by this criterion (though their adjustments are very small). These convergence criteria are relatively weak, but adequate for the present problem (see Sec. 3).

## 2.2. parameter choices

This section describes choices for the values of various parameters and quantities. The implications are discussed in Sec. 3, where the light curve fitting algorithm is applied to a simulated catalog of eclipsing binaries. Star 1 is defined to be the star at superior conjunction near phase zero, with the phasing arranged so that it is the one with the deeper eclipse. Using *dc* in mode 2 for detached binaries we find the surface potentials of stars 1 and 2, the orbital inclination, the temperature of star 1 (the temperature of star 2 is fixed), the orbital eccentricity, the luminosity of star 1 (the luminosity of star 2 is set by the other parameters), and an epoch of zero phase.

Since we do not know the temperatures, we use *dc* with the black body approximation.

We assume 10000 K for the temperature of star 2 (arbitrary choice) and a logarithmic limb darkening law. Explicitly (e.g. Van Hamme 1993) this law is written

$$D(\mu) = 1 - x(1 - \mu) - y\mu \ln \mu \quad (1)$$

where  $D(\mu = \cos \theta)$  is  $I(\mu)/I(\mu = 1)$  at a given surface point in a direction  $\theta$  with the normal. Intensities  $I$  refer to averages over a pass-band.  $x$  and  $y$  are the linear and non-linear limb-darkening co-efficients. From the colors reported in Udalski et al. (1998), the stars are expected to be primarily of O and B type. We therefore assume  $x = 0.32$  and  $y = 0.18$  respectively for both stars. The values are from Van Hamme 1993 for I-band, with an effective temperature of 15000K and  $\log g$  of 4.5 (*cgs*). We use the simple reflection model (Wilson, 1990), with a single reflection (MREF=1, NREF=1), and assume the stars have no spots. We also assume synchronous rotation, that bolometric flux is proportional to surface gravity, and a bolometric albedo of 1. The scatter of observations is assumed to scale with the square root of the flux level (parameter NOISE=1 in *dc*).

We assume that the initial argument of periastron,  $\omega_0$ , for star 1 (in radians) is constant in time, and that it takes a value of either 0 or  $\pi$ . This choice introduces systematic error into the solution for eccentricity and therefore into the stellar radii, and is particularly problematic where  $\omega_0 \approx \pm\pi/2$ . However the recovered eccentricity (and hence the radii) will be reasonable approximations in most cases since if  $\omega_0$  is distributed randomly, then for inclinations of 90 degrees, the projected position of periastron on the sky is distributed as  $1/|\sin\omega_0|$  (the results of the following section quantify this assertion). The mass ratio is assumed to be  $q = m_2/m_1 = 1$ , a choice that should be unimportant for well detached systems. There is an inherent ambiguity in partially eclipsing light curve fits between the radii of stars 1 and 2. That ambiguity may extend to complete eclipses for noisy light curves. When computing the library of light curve guesses, we assume that the hotter star (star 1) is larger, a choice that effectively restricts our solutions. We note that significantly evolved stars may not obey this condition. However the physically correct solution (which is essential for distance determination) will not usually be determined from photometry alone. The ambiguity must be resolved on a case by case basis with help from spectra. Importantly, the computation of a degenerate solution does not affect the selection of a particular binary as a potential distance indicator. Tests revealed that the OGLE systems typically have third-light consistent with zero, and we have accordingly set third light to zero in our photometric solutions. Lists of fixed and adjusted parameters (as well as those for which convergence was sought) and control integers are in Tabs. 1 and 2. Tab. 3 lists the two groups of subsets.

### 3. Application of the Fitting Procedure to Simulated Catalogs of Eclipsing Binaries

In this section we apply our light curve fitting algorithm to two simulated catalogs of eclipsing binaries. The first contains only detached binaries, while the other comprises semi-detached and over-contact systems. There are three objectives: 1) to quantify the applicability of the error estimates produced by  $dc$ , 2) to estimate the extent of the systematic error introduced by the assumption of fixed values for limb darkening coefficients, mass ratio, and argument of periastron, and 3) to estimate the success rate in finding good distance indicators. We generated 100 simulated detached eclipsing binaries having 150 randomly spaced observations (typical for OGLE eclipsing binaries) and Gaussian noise that scaled as square root of light with a level of 5% at the light curve mean. These systems have temperatures for star 2 of 15000K and for star 1 of between 15000K and 30000K. The temperature for star 2 differs from that assumed for real stars. We deliberately fit the wrong temperature to highlight the point that, although we do not know the temperatures of the real stars, the surface brightness ratio is the important quantity. The light curves were computed with logarithmic limb darkening coefficients corresponding to the temperatures (Van Hamme, 1993). The mass ratios ranged between 0.5 and 1, and  $\omega_0$  was randomly distributed. The simulated binaries were produced with assorted stellar potentials, orbital eccentricities and inclinations. Fig. 1 shows examples of the simulated light curve data, as well as computed light curves and residuals obtained with the fitting algorithm outlined in Sec. 2. Our algorithm found a converged solution with residuals comparable to the scatter for 95% of cases.

We refer to the radius toward the center of mass as the point radius ( $R$ ). Radii are quoted as fractions of the stellar separation ( $a$ ). The top panels of Fig. 2 show radii of star 1 ( $r_1 \equiv R_1/a$ , left) and of star 2 ( $r_2 \equiv R_2/a$ , right) found from the light curve solution (with standard error,  $\Delta r$ ) plotted against the known values for the simulated binaries ( $r_{sim}$ ). The line of equality is also drawn to guide the eye. The plot demonstrates that the fitting scheme does an excellent job of recovering input model radii, and that the errors provide a good description of solution accuracy (including systematic uncertainty). This is further demonstrated by the lower panels of Fig. 2 that show  $|r - r_{sim}|/\Delta r$  plotted against the absolute size of the error  $\Delta r$ . Naturally there is some tendency for the solutions with larger errors to be closer (in units of standard error) to the correct value. However the errors are surprisingly normal over the full range of error sizes, and do not exhibit a large tail.

Fig. 3 shows the solution values (with standard errors) plotted against simulated values for  $r_1 + r_2$ ,  $r_1/r_2$ , surface brightness ratio ( $\frac{J_1}{J_2}$ ), luminosity ratio ( $\frac{L_1}{L_2}$ ), inclination, and eccentricity. The sum of radii is very accurately reproduced, while the surface brightness ratio

is also reliably recovered. For surface brightness ratios near 1, the solution has a relatively small uncertainty, although the standard errors are realistic over the range. While the inclination is not recovered accurately, the standard errors are again representative. However significant error is clearly present in some solutions for the ratio of radii, and the ratio of luminosities for some systems. The eccentricity is often not recovered, and has unrealistic standard errors because the error is completely dominated by the systematic error introduced by the assumption that  $\omega_0$  is 0 or  $\pi$ . The fitted eccentricity is a lower limit.

The relatively large uncertainties in the ratio of radii and inclination can be traced to the following: In the case of partial eclipses, a change in the ratio of radii can nearly be compensated (with regard to eclipse depth) by a change in inclination, so there is a near-degeneracy between the ratio of radii and the inclination. This degeneracy may be broken if the eclipses are complete, and we thus expect smaller errors for the individual radii in these cases. Turning this around, solutions with small relative errors in the radii can therefore be used to determine whether a binary is completely eclipsed. We define the quantity:

$$F_e \equiv \frac{r_{p,1} + r_{p,2} - \cos i}{2r_{p,2}}, \quad (2)$$

which is greater than 1 for systems with complete eclipse (strictly true only for spherical stars, but nearly true otherwise). Here the  $r_p$  are the polar radii in units of orbital semi-major axis,  $a$ . The left panel of Fig. 4 shows  $F_e$  for the simulated binaries plotted against the corresponding values from the light curve solution. Lines of unity are drawn to separate regions of complete and incomplete eclipse for both the simulated binaries and their solutions. Due to the large uncertainties in inclination and ratio of radii, the solution  $F_e$ 's are also very uncertain. The right panel of Fig. 4 shows the number of standard errors ( $\Delta F_e$ ) by which the solution for  $F_e$  differs from its correct value plotted against the absolute size of the error. This plot demonstrates that while  $F_e$  is not recovered accurately in most cases, the standard errors are realistic. Cases where  $\Delta r_1/r_1 < 0.05$  and  $\Delta r_2/r_2 < 0.05$  are denoted by larger dots and have their standard error bars shown (left panel). The solutions for this subset of systems recover  $F_e$  (sometimes accurately) with realistic standard errors.

Since many of the OGLE binaries are not detached, simulated catalogs of semi-detached (mode 5) and over-contact (mode 1) binaries were produced by applying noise and sampling to model light curves as before. In the case of semi-detached binaries the potential of star 2 was fixed by the mass ratio. For the over-contact binaries the potential of star 2 was equal to the potential of star 1. Our detached binary fitting algorithm was unable to converge to a solution for any of the over-contact systems. This failure is expected and is a consequence firstly of the fact that the over-contact light curve geometry cannot typically be produced from a detached system, and secondly that we have assumed  $q = 1$ . Whilst the assumption

of  $q = 1$  is reasonable when discussing detached systems, over-contact binaries have light curves that are sensitive to  $q$ , which is nearly always far from 1. However detached solutions were found for about two thirds of semi-detached binaries (the somewhat low success rate can again be traced to the fixed  $q$ ). Because the simulated semi-detached catalog was produced in mode 5, the cooler star (star 2) fills its critical lobe. The radius is therefore typically larger for star 2 than for star 1. However our procedure provides an initial guess having a radius that is larger for star 1 than for star 2. Solutions can be nearly ambiguous between cases where the radii but not the temperatures are interchanged. Since star 1 is defined to be hotter and we start from an assumption that  $R_1 > R_2$ , we may find this alternate (incorrect) solution for many SD systems when they are solved as detached. Importantly, where a fit is obtained the sum of the radii and the surface brightness ratio are recovered accurately, and with realistic errors. Over-contact and semi-detached systems should therefore not contaminate our selection of well detached distance indicators.

In summary, we find the following: The assumption of an  $\omega_0$  that is either 0 or  $\pi$  radians can introduce significant systematic error into the solution for eccentricity. The resulting systematic contributions to the errors in radii from the limb darkening, argument of periastron and the uncertainty in surface brightness ratio often render the solution for luminosity ratio incorrect, and with unrealistically small error bars. However the  $r$ 's, their sum, and the surface brightness ratio are reliably reproduced. Furthermore, solutions having a small relative error in both radii accurately determine  $F_e$ , and therefore whether the binary undergoes total eclipse.

#### 4. Application of the Fitting Procedure to the OGLE Catalog of Eclipsing Binaries in the SMC

We next applied our algorithm to the OGLE SMC eclipsing binary catalog. We obtained solutions for  $\sim 80\%$  of binaries. Given our high success rate on the simulated catalogs, we infer that the remaining  $\sim 20\%$  are predominantly in semi-detached or over-contact condition. Another possibility is that some of the un-fitted systems have mass ratios very different from 1, with one star having a normalized radius greater than one half. Not all our detached solutions necessarily imply a detached system. Due to the typical noise levels, a detached solution with  $q = 1$  may be found for a semi-detached light curve having  $q \neq 1$ . However, these systems will have at least one large component. The OGLE SMC eclipsing binary catalog has 68 objects that are in two overlapping fields. As a check we found solutions for these objects using both data sets. In these cases we find consistent solutions.

Figure 5 shows 27 examples (from OGLE field smc-sc2) of light curve fits and residuals,

as well as 3 examples where no solution was found because an iteration moved outside the physical bounds of the  $q = 1$  detached system. The latter have light curves that are strongly rounded outside the eclipses, indicative of a semi-detached or over-contact condition. Figs. 6 and 7 summarize the solution parameters in the OGLE SMC fields. The figures demonstrate the range of solutions and also the range of solution quality. The figures show  $r_1$  vs.  $r_2$  (Fig. 6) and  $r_1 + r_2$  vs. surface brightness ratio (Fig. 7). Points for all systems are shown, but for clarity only  $r_{1,2}$  error bars smaller than 0.05, surface brightness ratio error bars smaller than 0.25, and  $r_1 + r_2$  error bars smaller than 0.1 are shown. Systems that will be useful distance indicators are principally found in the lower left regions of both plots.

#### 4.1. a sub-catalog of systems suitable for distance determination

We have quantitatively selected two catalogs of objects that should be particularly reliable distance indicators:

##### 4.1.1. well separated systems

The first catalog is composed of systems having a small and well determined  $r_1 + r_2$ , similar temperatures, and deep eclipses. These well detached systems have the advantage that the surface brightness - temperature relation can more easily be calibrated empirically. In particular, in relation to surface brightness, well detached systems can be considered as two isolated stars. The surface brightness - temperature relation can therefore be measured for isolated stars as well as eclipsing binaries. Fig. 8 shows a collection of light curve fits for the best well detached systems for distance determination. Their parameters are in Tab. 4. They have  $r$ 's smaller than 0.2, surface - brightness ratios smaller than 1.5, and sufficiently high inclinations so that one eclipse depth is larger than 0.25 of the maximum light curve flux (measured from the light curve solution). In addition the standard errors in radii are smaller than 0.05, the standard errors in surface brightness ratio are smaller than 0.25, and the standard errors in the inclination are smaller than 10 degrees. The systems are evenly distributed across the OGLE fields.

Fig. 9 shows color - period and color - magnitude diagrams for the selected objects superimposed on the full catalog of OGLE SMC eclipsing binaries. The V-I colors have been de-reddened assuming the average reddening of field stars for the SMC  $E(V-I)=0.14$  (Massey, Lang, DeGioia-Eastwood & Garmany 1995). The potential distance indicators fall into two classes according to period. The great majority have periods of a few to 10 days,

with colors and magnitudes consistent with their being O, B or A stars. Most of these short period binaries are noticeably fainter than the brightest blue binaries in the OGLE catalog, suggesting that they might be B or A rather than O stars. B-type (and cooler) components are typically more desirable for distance determination than are O stars since their spectra do not usually contain emission lines or other peculiarities. B stars also are less likely than O stars to have winds that contaminate the radial velocity determination, although spectra are required to establish suitability on these grounds. A further important consideration is the surface brightness - temperature relation, which one may want to calibrate empirically for the least controversial distance determination. The list of candidates for this calibration compiled by Kruszcwski & Semeniuk (1999) from the Hipparcos catalog contains no O stars. Existing calibrations (e.g. Di Benedetto 1998; van Belle et al. 1999) are primarily for later spectral types.

A second, much rarer class (objects smc-sc9 55949 and smc-sc10 137844) have longer periods of tens to hundreds of days, and significantly redder colors, consistent with G or K stars. One of these (smc-sc10 137844) has a luminosity consistent with its components being of class II, very smooth residuals, and the smallest standard errors of any of the solutions in Tab. 4. In addition to the original solutions, we obtained solutions for these red objects assuming more appropriate limb darkening coefficients ( $x = 0.60$ ,  $y = 0.21$ , from Van Hamme 1993 for an effective temperature of 5000K and a  $\log g$  of 4.5). The results are given in parentheses in Tab. 4 and show that the two solutions are consistent to within standard error. These are rare and potentially very interesting objects. They will have low radial velocity amplitudes, therefore requiring higher dispersion spectra. However they are bright, and being of a cooler spectral type, will have many spectral lines. Furthermore, the surface brightness - temperature relation is empirically well established over the range of spectral types A to K (Di Benedetto 1998; van Belle et al. 1999), and is nearly parallel to the reddening line for late type stars (Barnes & Evans 1976). We note that none of the systems selected as well detached distance indicators have very short periods ( $< 2$  days).

#### *4.1.2. systems exhibiting complete eclipse*

A second catalog contains detached systems with small relative errors in individual radii, similar temperatures, and complete eclipses. These systems have the advantage that the photometric solutions may often provide good determinations of inclination, or at least a robust lower limit. Fig. 10 shows the 29 light curve fits whose parameters are in Tab. 5. The systems have  $\Delta r/r$ 's smaller than 0.05, surface-brightness ratios smaller than 1.5, standard errors in surface brightness ratio smaller than 0.25, and sufficiently high inclinations so that

one eclipse depth is larger than 0.25 of the maximum light curve flux (measured from the light curve solution). Instances of complete eclipse were determined from  $F_e$ . The solutions yield either  $F_e > 1$  and  $\Delta F_e < 0.05$  or  $F_e > 1.1$  and  $\Delta F_e < 0.1$ . These systems are again evenly distributed across the OGLE fields.

Fig. 11 shows color - period and color - magnitude diagrams for the selected objects superimposed on the full catalog of OGLE SMC eclipsing binaries. The V-I colors have been de-reddened assuming  $E(V-I)=0.14$  as before, and the systems follow a distribution in color - magnitude space similar to those in the well detached catalog. Two of the binaries (smc-sc4 75638 and smc-sc10 137844) are significantly redder than the main group. smc-sc10 137844 also appeared in the well detached catalog described in the previous sub-section, and the second solution of Tab. 4 is reproduced in Tab. 5. We also obtained a second solution for smc-sc4 75638 assuming more appropriate limb darkening coefficients ( $x = 0.39$ ,  $y = 0.20$ , from Van Hamme 1993 for an effective temperature of 10000K and a  $\log g$  of 4.5). These two solutions are consistent to within standard error. In addition to smc-sc10 137844, smc-sc5 129441 also appears in both catalogs. These two binaries are marked by daggers in Tabs. 4 and 5 and are very special, each having a complete eclipse and small, similar components.

#### 4.1.3. *solutions for the Udalski et al. (1998) potential distance indicators*

Udalski et al. (1998) selected objects suitable for distance determination on the basis of being bright with good photometry and having deep and well defined eclipses. For this catalog Fig. 12 shows  $r_2$  plotted against  $r_1$  (left) as well as  $r_1 + r_2$  plotted against surface brightness ratio (right). Only standard errors in  $r$  smaller than 0.05, in  $r_1 + r_2$  smaller than 0.1, and in surface brightness ratio smaller than 0.25 are plotted. Most of these objects have  $r$ 's greater than 0.25. At that size they will be tidally distorted and so may not be ideal as distance indicators since their empirically calibrated surface brightness - temperature relations may not be accurate. However, many of the systems with larger components exhibit complete eclipses. About half of our samples (marked with \* in Tabs. 4 and 5) are in the Udalski et al. (1998) compilation. Many of these are among the most desirable due to their brightness, but the Udalski et al. (1998) catalog is missing many of the best systems. This point illustrates the need for quantitative selection.

## 5. Conclusion

We have developed an automated procedure for finding solutions to eclipsing binary light curves and applied it to the light curves of the 1459 eclipsing binaries found in the central 2.4 square degrees of the SMC by the OGLE collaboration (Udalski et al. 1998). We find detached solutions for  $\sim 80\%$  of these, though many systems are found to have large components and may be semi-detached. By fitting simulated catalogs we estimate a 95% success rate in finding acceptable converged solutions to detached systems. We extracted two sub-catalogs of systems that should make especially good distance indicators. The first is based on small, well determined fractional radii and surface brightness ratios. The second contains systems whose solutions provide accurate radii and indicate complete eclipses. Two binaries are in both catalogs and therefore are the leading candidates. One of these comprises two G-type, class *II* giants.

The next step is to obtain spectra so as to identify the most suitable systems on the basis of spectral type. Improved multi-band light curves should then be observed. In addition, reliable distance indicators require well determined reddening (e.g. Gibson 1999; Popowski 2000). Planned observations will address these issues.

The authors are very grateful to Professor Bohdan Paczynski for suggesting this project, as well for his continual encouragement and helpful comments on the manuscript. We would like to thank Professor Slavek Rucinski for comments on a draft version of the manuscript. We would also like to thank the referee Dr I. Ribas for a careful reading of our paper. Finally we are indebted to the OGLE collaboration for making their data public domain, and hence projects like this possible. This work was supported in part by NSF grants AST-9819787 and AST-9820314 to Professor Paczynski. JSBW acknowledges the support of an Australian Postgraduate Award.

## REFERENCES

- Alcock, C. et al., 1997, *Astron. J.*, 114, 326  
Andersen, J., 1991, *Astron. Astrophys. Rv.*, 3, 91  
Barnes, T. G. & Evans, D. S., 1976, *MNRAS*, 174, 489  
Di Benedetto, G.P, 1998, *Astron. Astrophys*, 339, 858  
Fitzpatrick, E.L., Ribas, I., Guinan, E.F., DeWarf, L.E., Maloney, F.P., Massa, D., 2001, *ApJ*, in press, astro-ph/0010526

- Freedman W. L. et al., 2001, ApJ, in press, astro-ph/0012376
- Gibson, B. K., 1999, in Mem. Soc. Astron. Italiana (MemSAI), astro-ph/9910574
- Grison, P. et al., 1995, Astron. Astrophys. 109, 447
- Guinan et al., 1998, Ap. J., 509, 21
- Kruszewski, A., Semeniuk, I., 2000, AcA, 49, 561
- Lacy, C.H., 1979, Ap.J., 228, 817
- Levenberg, K., 1944, Quarterly of Applied Mathematics, 2, 164
- Marquardt, D. W., J. Soc. Indust. Appl. Math., 11,431
- Massey, P., Lang, C.C., DeGioia-Eastwood, K., Garmany, C.D., 1995, ApJ, 438, 188
- Paczynski, B., 2000, Millennium Essay, Publications of the Astronomical Society of the Pacific, astro-ph/0005284
- Paczynski, B., 1997, Invited talk, presented at The Extragalactic Distance Scale STScI May Symposium, astro-ph/9608094
- Popowski, P., 1999, ASP Conference Series, 203, 201, astro-ph/0001545
- Semeniuk, I., 2000, AcA, 50, 381
- Udalski, A., et al., 1998 AcA, 48, 563
- Van Hamme, W., 1993, AJ, 106, 2096
- Van Belle, G.T., 1999, Astron. J., 117, 521
- Wilson, R. E., 1979, Ap. J., 234, 1054
- Wilson, R. E., 1990, Ap. J., 356, 613
- Wilson, R. E., 1998, “Computing Binary Star Observables”, Department of Astronomy, University of Florida, Gainesville, FL, 1998 edition
- Wilson, R. E., 2001, IBVS, No. 5076
- Wilson, R. E., Biermann, P., 1976, Astron. Astrophys, 48, 349
- Wilson, R. E., Devinney, E. J., 1971, Ap. J., 166, 605

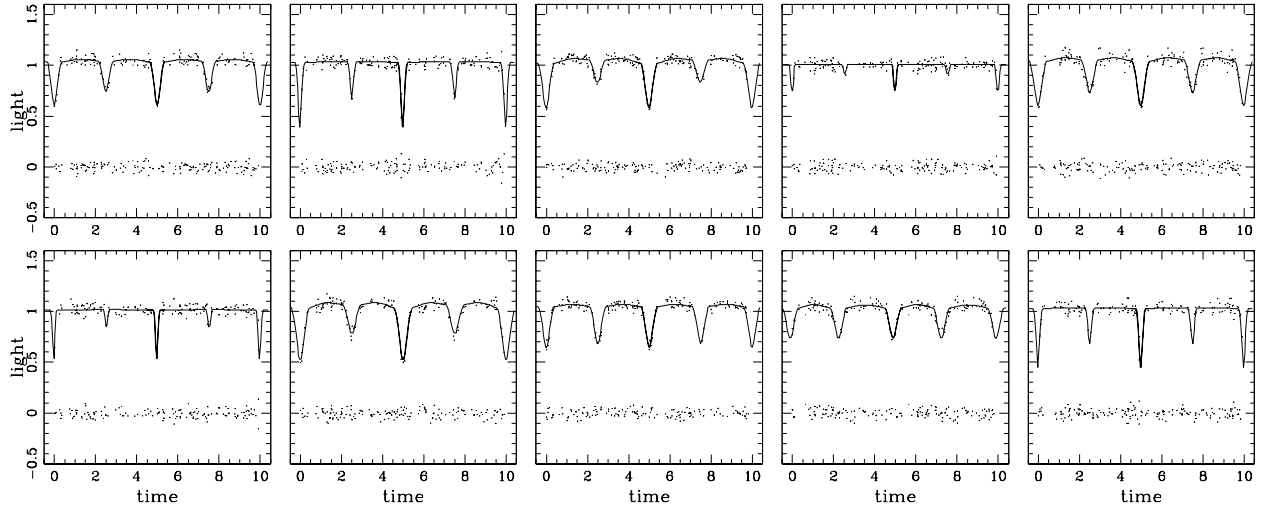


Fig. 1.— Examples of the simulated light curve data with corresponding light curve solutions and residuals.

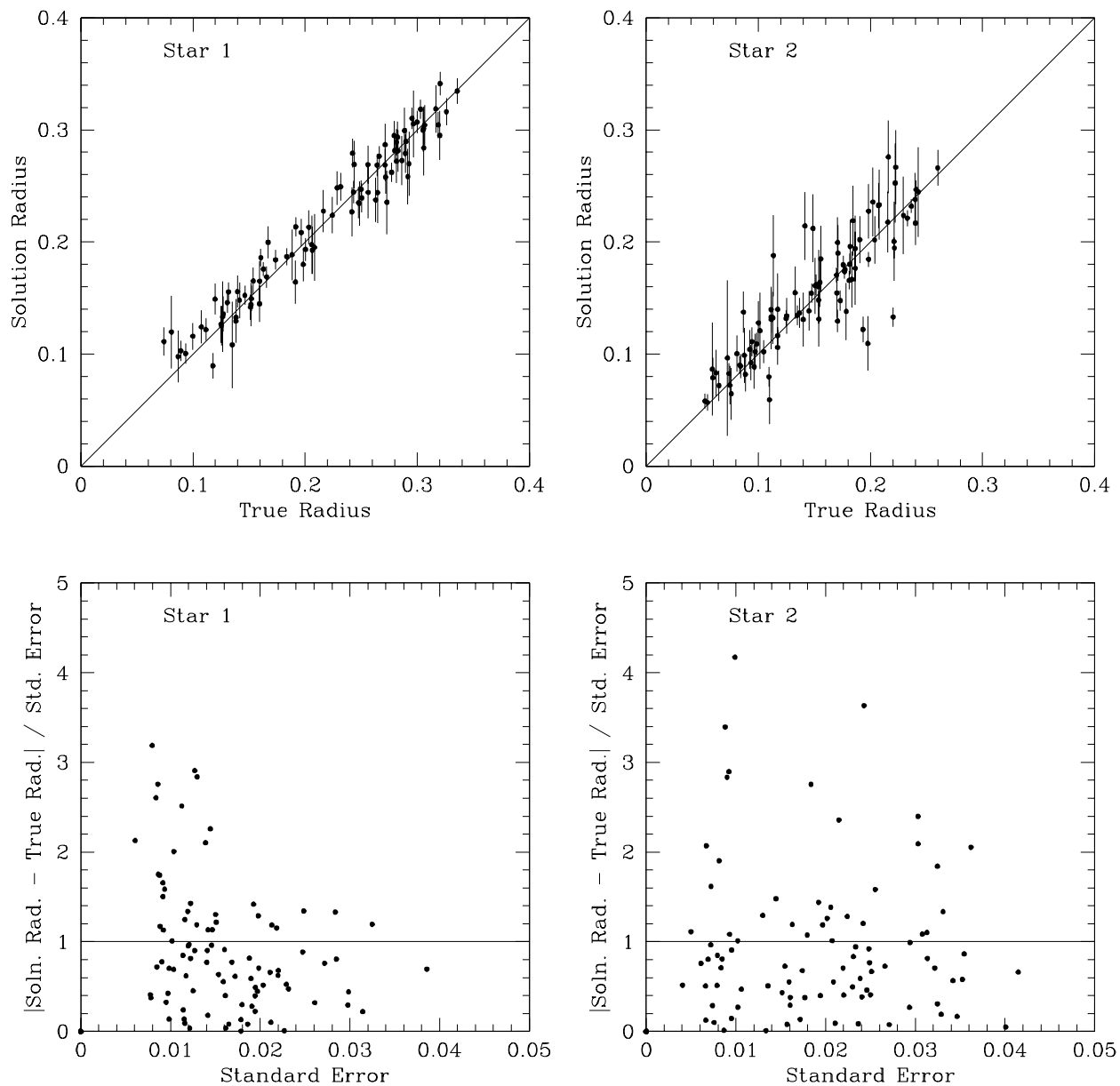


Fig. 2.— Top: Values for the radius ( $r$ ) of Star 1 (left) and the radius of Star 2 (right) (with standard error,  $\Delta r$ ) found from the light curve solution plotted against the values ( $r_{sim}$ ) for the simulated detached eclipsing binaries. The line of equality is also drawn to guide the eye. Bottom:  $|r - r_{sim}|/\Delta r$  plotted against the standard error  $\Delta r$ . (Left: Star 1, Right: Star 2).

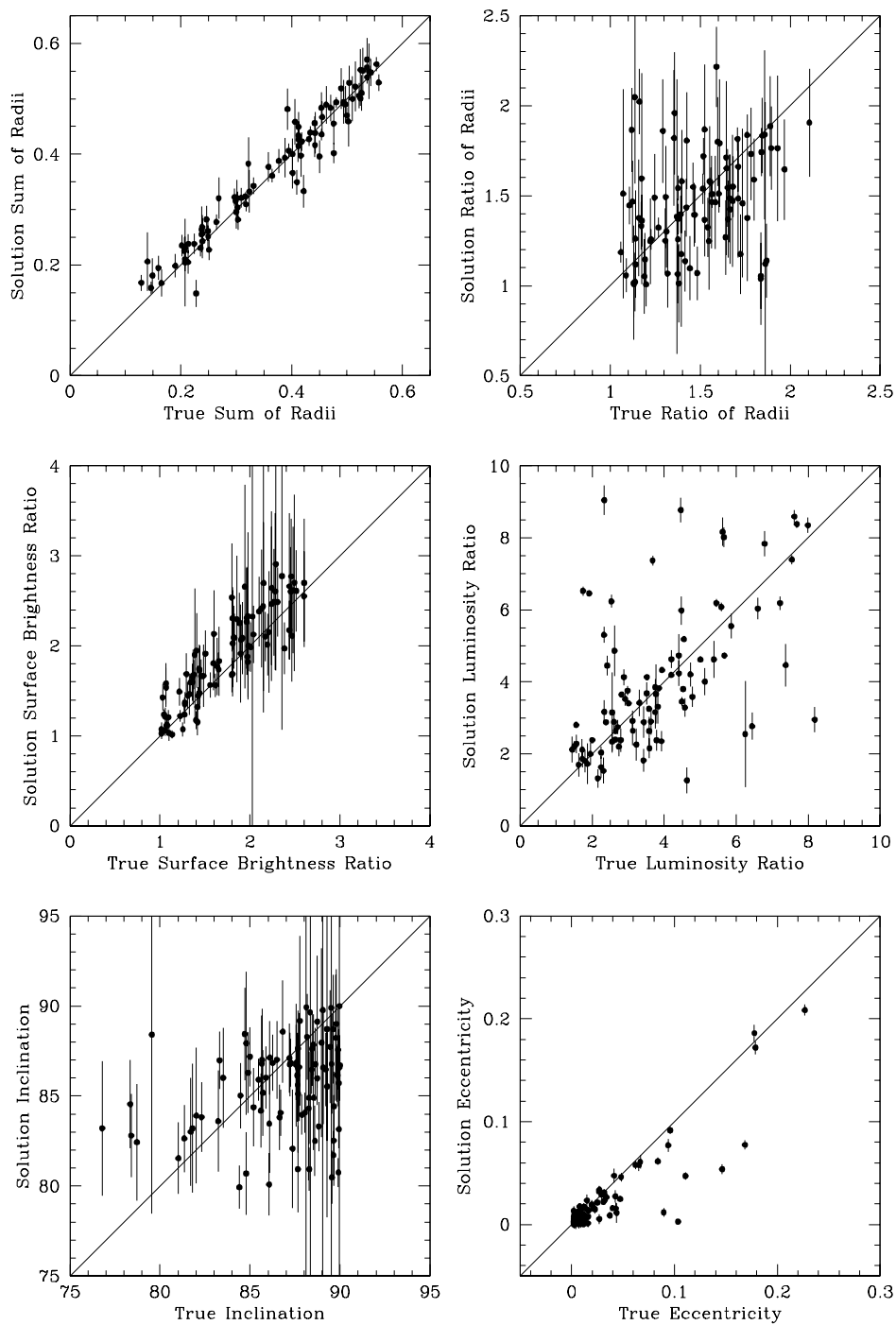


Fig. 3.— Values for the light curve solution (with standard errors) plotted against the values for the corresponding simulated binary parameters. Plots are shown for the following parameters: the sum of the radii, the ratio of radii, the ratio of surface brightness, the luminosity ratio, the inclination, and the eccentricity.

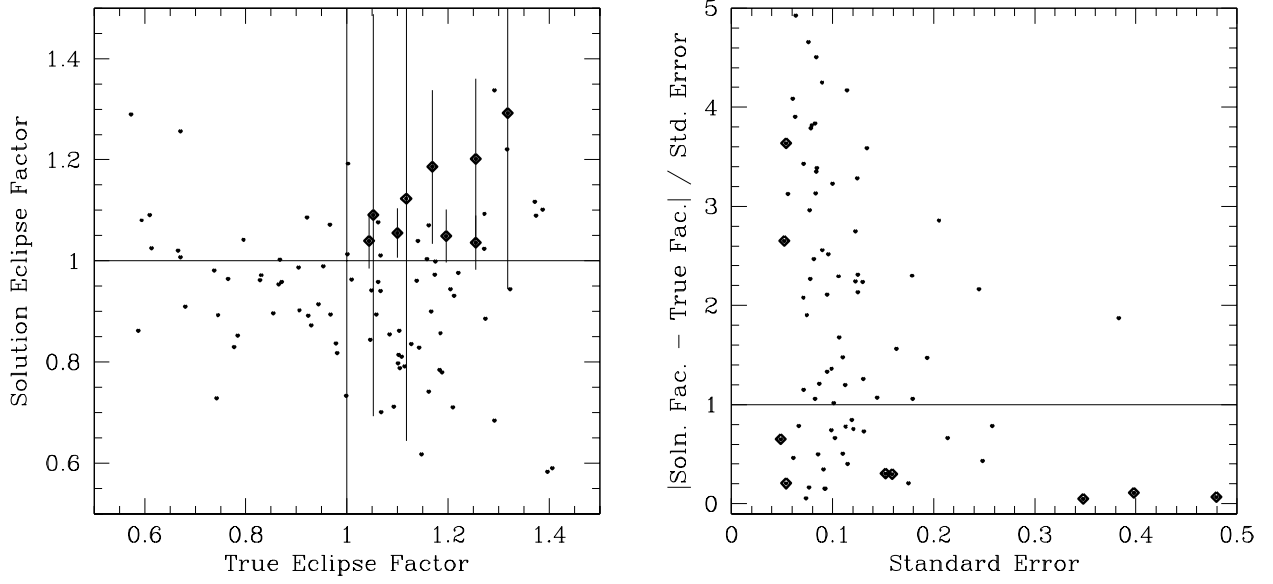


Fig. 4.— Left: Values of  $F_e$  found from the light curve solution plotted against the values for the simulated detached eclipsing binaries ( $F_{sim}$ ). The lines of unity are also drawn to separate regions of complete and incomplete eclipse. Right:  $|F_e - F_{sim}|/\Delta F_e$  plotted against the standard error ( $\Delta F_e$ ). Cases where  $\Delta r_1/r_1 < 0.05$  and  $\Delta r_2/r_2 < 0.05$  are denoted by larger dots and have their standard error bars shown (left panel).

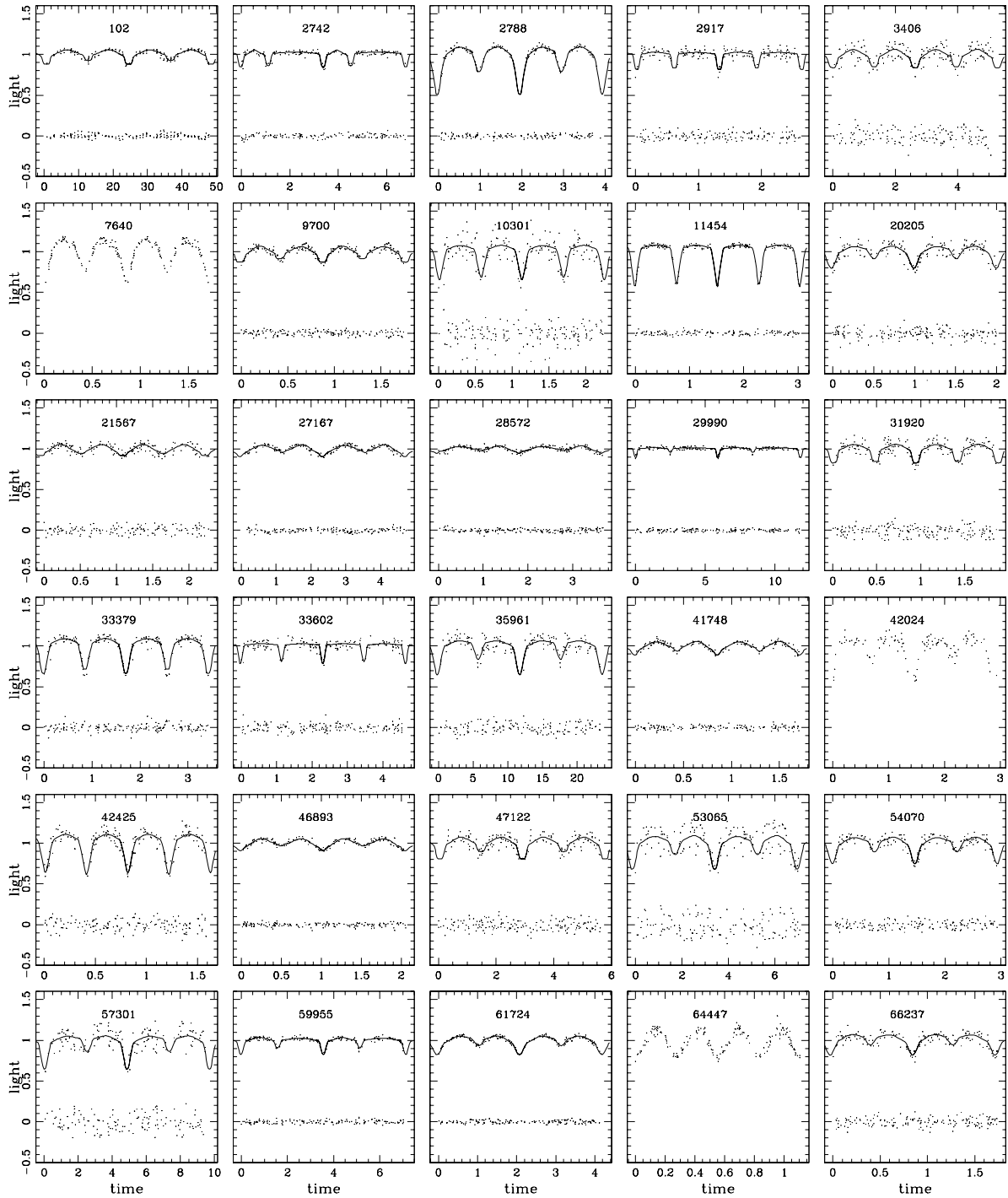


Fig. 5.— Examples from OGLE field smc-sc2 of light curve solutions with residuals, as well as systems where no solution was found (objects 7640, 42024 and 64447). Each panel is labeled by the OGLE object identification number.

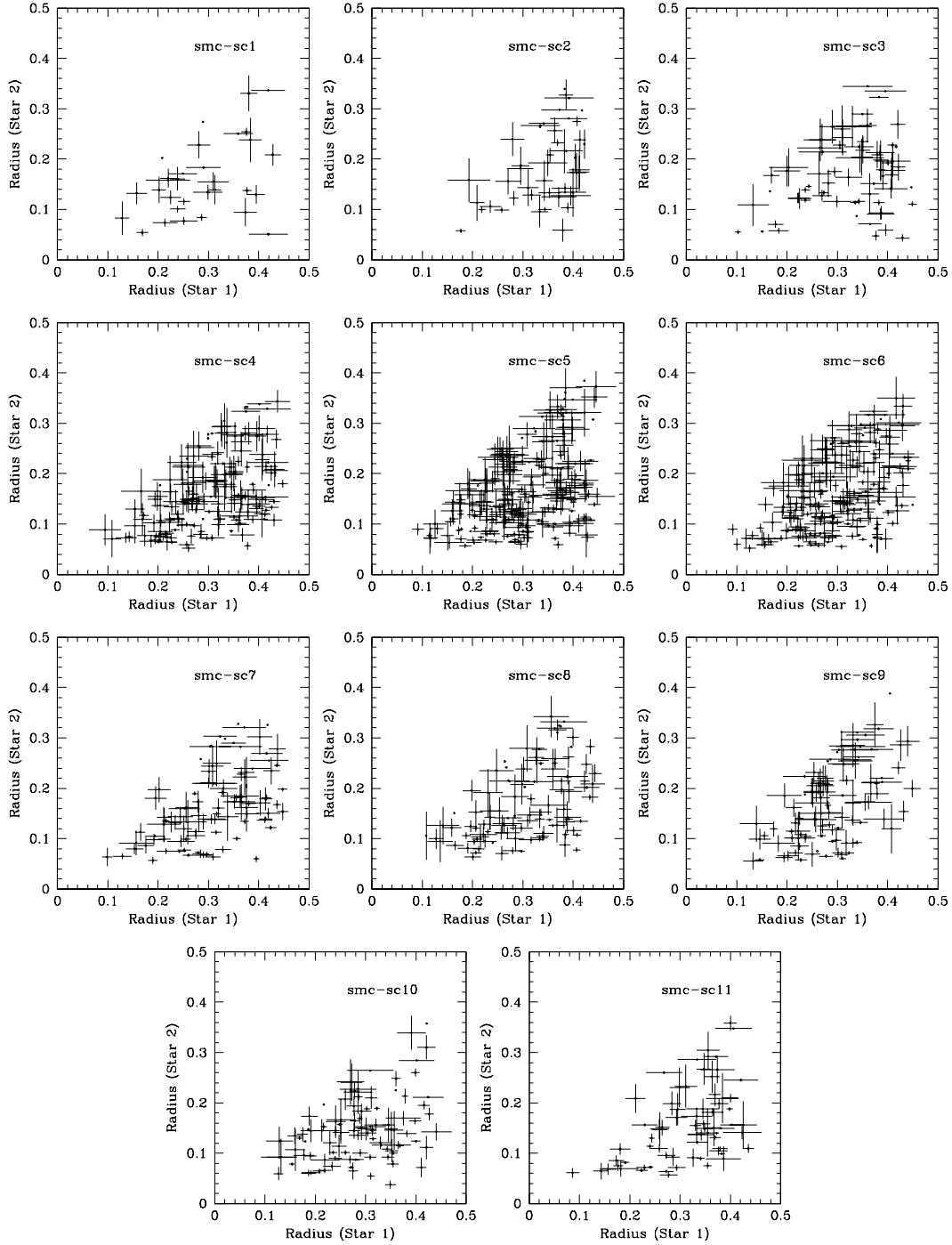


Fig. 6.— Solutions for the radius of Star 1 plotted against the solutions for radius of Star 2. Only error bars smaller than 0.05, are shown.

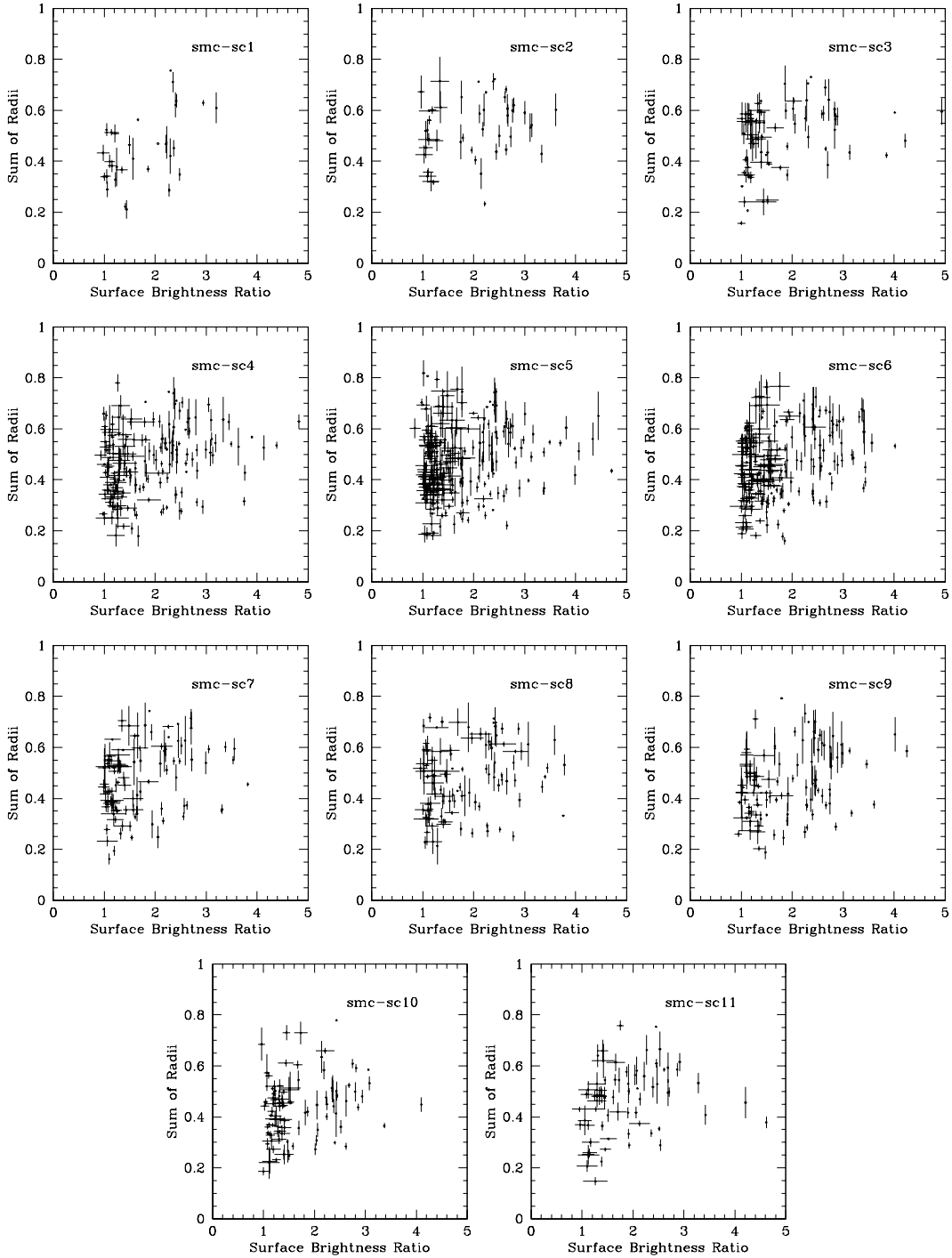


Fig. 7.— Solutions for the sum of the radii plotted against the solution for surface brightness ratio. Only error bars in surface brightness ratio smaller than 0.25, and in the sum of the radii smaller than 0.1 are shown.



Fig. 8.— A collection of light curve solutions for well detached OGLE eclipsing binaries which will make the best systems for distance determination. Each panel is labeled by the OGLE field and object identification numbers. The solution parameters are given in Tab. 4

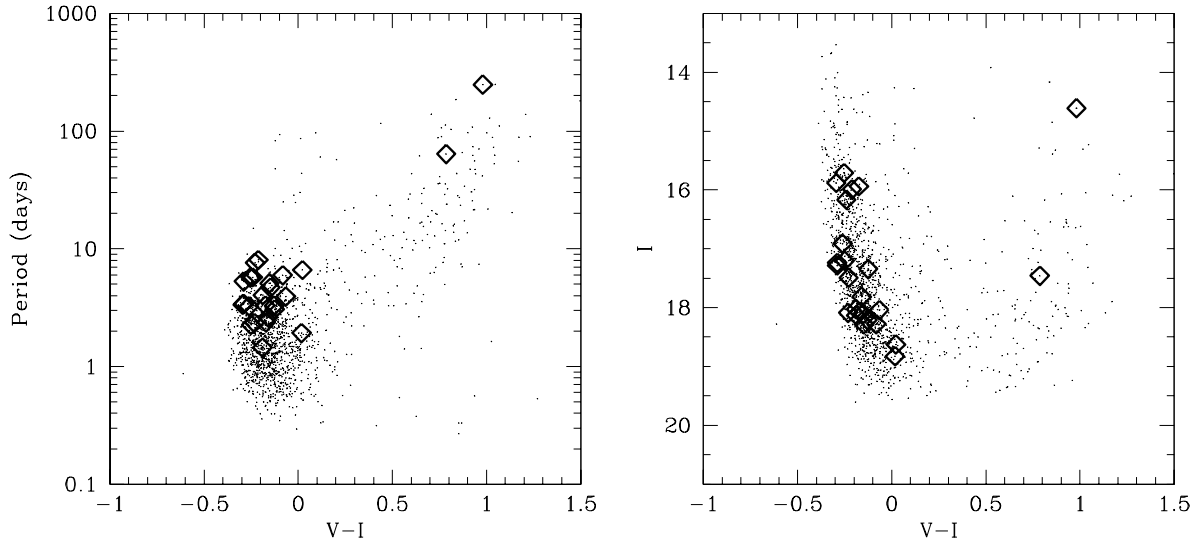


Fig. 9.— Color - period and color - magnitude diagrams for the complete eclipsing binary catalog (small dots, data from Udalski et al. 1998). The well detached objects selected as potential distance indicators are superimposed (diamonds). The V-I colors have been de-reddened assuming  $E(V-I)=0.14$ .

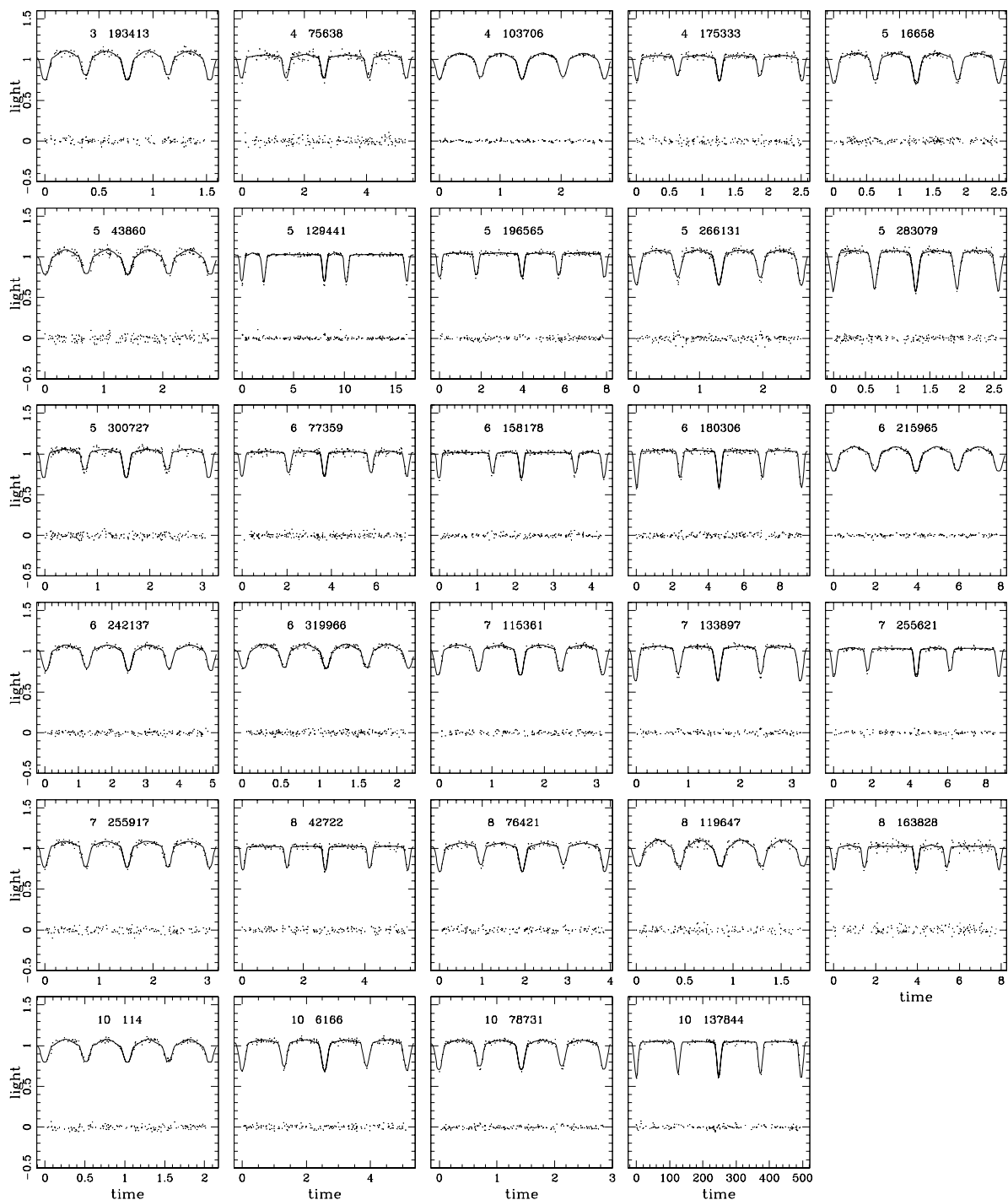


Fig. 10.— A collection of light curve solutions for OGLE eclipsing binaries exhibiting complete eclipse. Each panel is labeled by the OGLE field and object identification numbers. The solution parameters are given in Tab. 5

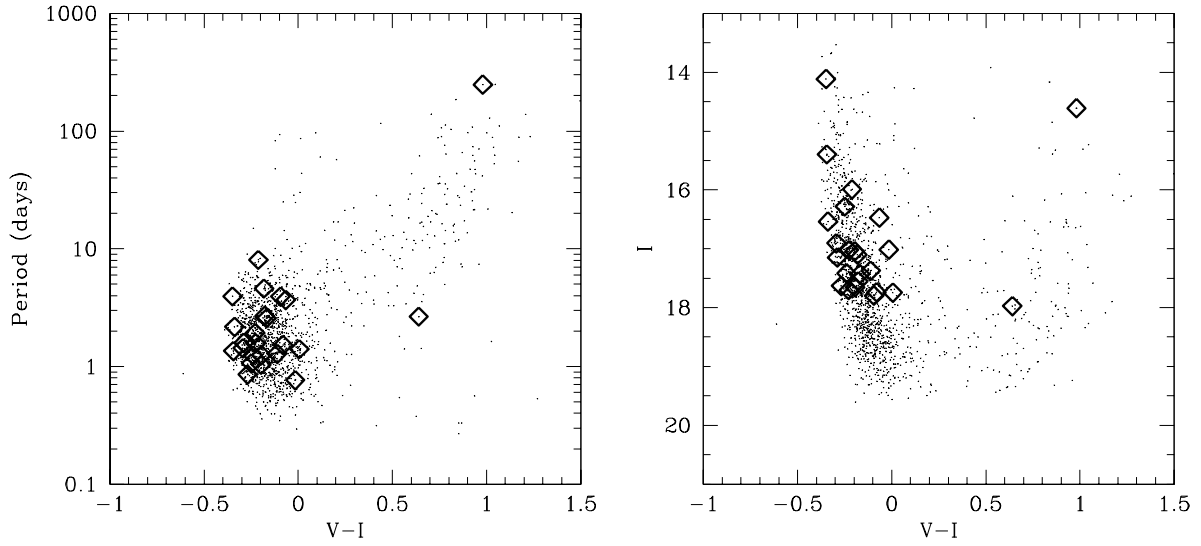


Fig. 11.— Color - period and color - magnitude diagrams for the complete eclipsing binary catalog (small dots, data from Udalski et al. 1998). The objects selected to have complete eclipses are superimposed (diamonds). The V-I colors have been de-reddened assuming  $E(V-I)=0.14$ .

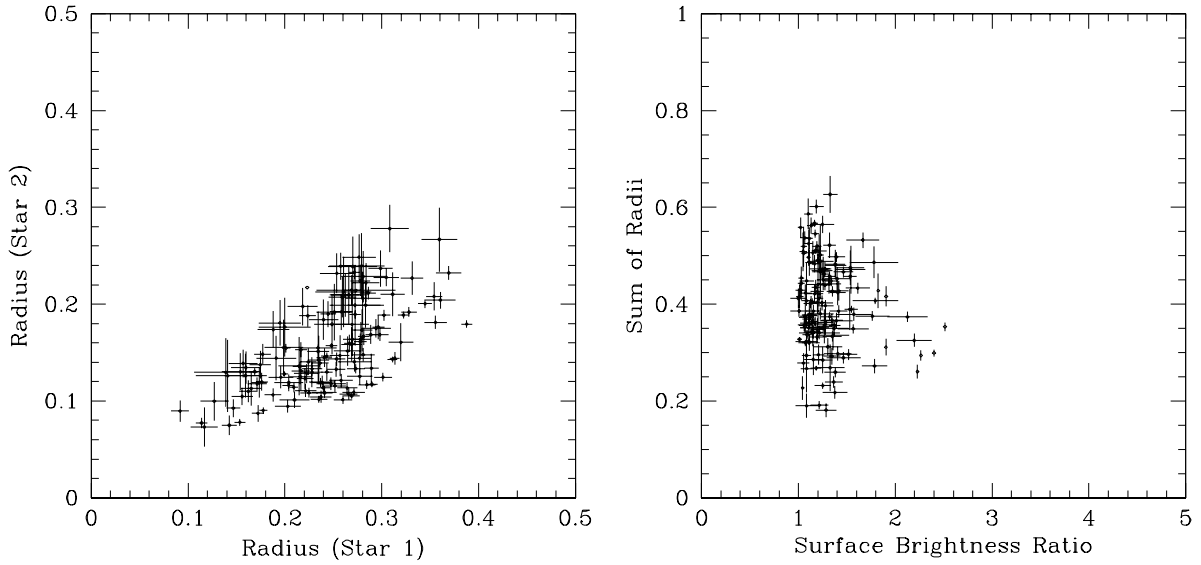


Fig. 12.— Solutions for the collection of distance indicators compiled by Udalski et al. (1998). Left: Solutions for the radius of Star 2 plotted against the solutions for the radius of Star 1. Only standard errors smaller than 0.05, are shown. Right: Solutions for the sum of the radii plotted against the solutions for surface brightness ratio. Only standard errors in surface brightness ratio smaller than 0.25, and in the sum of the radii smaller than 0.1 are plotted.

parameter	description
$i$ (adjusted*)	binary orbit inclination.
$T_1$ (adjusted*)	mean surface effective temp. (K) of star 1.
$L_1$ (adjusted*)	luminosity for star 1.
$\Omega_1$ (adjusted*)	potential of star 1.
$\Omega_2$ (adjusted*)	potential of star 2.
$T_0$ (adjusted)	zero point of orbital ephemeris.
$e$ (adjusted)	binary orbit eccentricity.
$q = 1.0$	mass ratio.
$T_2 = 10000.0$	mean surface effective temp. (K) of star 2.
$L_2$ (set from initial guess)	luminosity for star 2.
$P$ (from Udalski et al.)	period of binary orbit.
$\dot{P} = 0.0$	first derivative of orbital period.
$\omega_0 = 0.0$ or $\pi$	initial argument of periastron for star 1.
$\dot{\omega}_0 = 0.0$	time derivative of $\omega_0$ .
$\lambda_I = 0.9$	wavelength of light curve in microns.
$x_1 = 0.32$	linear limb darkening coefficient of star 1.
$x_2 = 0.32$	linear limb darkening coefficient of star 2.
$y_1 = 0.18$	non-linear limb darkening coefficient of star 1.
$y_2 = 0.18$	non-linear limb darkening coefficient of star 2.
$l_3 = 0.0$	third light.
$f_1 = 1.0$	ratio of axial rotation rate to mean orbital rate.
$f_2 = 1.0$	ratio of axial rotation rate to mean orbital rate.
$g_1 = 1.0$	exponent in gravity brightening (bolo. flux prop. to local gravity).
$g_2 = 1.0$	exponent in gravity brightening (bolo. flux prop. to local gravity).
$A_1 = 1.000$	bolometric albedo of star 1.
$A_2 = 1.000$	bolometric albedo of star 2.
$\lambda = 10^{-5}$	the Marquardt multiplier.

Table 1: Table of parameters with descriptions. The adjusted parameters are labeled as such (those for which convergence is required are also marked by \*), and the values of fixed parameters are given. Note that  $g$  should not be confused with surface gravity.

control integer	description
nref = 1	number of reflections.
mref = 1	simple reflection treatment.
ld = 2	logarithmic limb darkening law.
jdphs = 1	independent variable time.
noise = 1	scatter scales with sqrt level.
mode = 2	mode of program operation.
ipb = 0	for normal operation in mode 2.
ifat1 = 0	for black body (star 1).
ifat2 = 0	for black body (star 2).
n1 = 30	grid size for star 1.
n2 = 30	grid size for star 2.
N1L = 15	coarse grid integers for star 1.
N2L = 15	coarse grid integers for star 2.
IFVC1 = 0	no radial velocity curve for star 1.
IFVC2 = 0	no radial velocity curve for star 2.
NLC = 1	number of light-curves.
KDISK = 0	no scratch pad.
ISYM = 1	use symmetrical derivatives.

Table 2: Table of control integers with descriptions (nomenclature from Wilson 1998).

Group 1		
subset 1	subset 2	subset 3
$e$	$i$	$T_1$
$\Omega_1$	$L_1$	$T_o$
$\Omega_2$		

Group 2		
subset 1	subset 2	subset 3
$e$	$i$	$T_1$
$T_o$	$\Omega_2$	$\Omega_1$
$L_1$		

Table 3: Table showing the two groups of subsets used by dc.

Field	Object	Radius of star 1 $\frac{R_1}{a}$	Radius of star 2 $\frac{R_2}{a}$	Surf.-bright. ratio $\frac{J_1}{J_2}$	inclination $i$ (degrees)	eccentricity $e$	Period (days)	I	B-V	V-I
3	157431	0.133 ± 0.032	0.109 ± 0.042	1.435 ± 0.248	84.3 ± 1.7	0.005 ± 0.003	2.37674	18.071	-0.042	-0.031
4	19130	0.153 ± 0.021	0.097 ± 0.035	1.263 ± 0.222	84.7 ± 2.3	0.007 ± 0.004	5.95288	18.280	0.002	0.058
4	23166	0.095 ± 0.032	0.088 ± 0.031	1.226 ± 0.180	89.6 ± 6.2	0.002 ± 0.002	4.04442	18.132	-0.109	-0.048
4	26278*	0.199 ± 0.020	0.155 ± 0.029	1.268 ± 0.085	86.4 ± 2.3	0.007 ± 0.003	3.06268	17.343	-0.029	0.015
4	54029*	0.154 ± 0.020	0.130 ± 0.019	1.253 ± 0.100	85.0 ± 0.9	0.104 ± 0.002	2.61830	17.815	-0.038	-0.020
5	129441*†	0.199 ± 0.004	0.128 ± 0.003	1.012 ± 0.026	87.3 ± 0.8	0.375 ± 0.001	8.05053	15.991	-0.128	-0.071
5	180516*	0.114 ± 0.006	0.077 ± 0.005	1.216 ± 0.093	88.4 ± 1.0	0.037 ± 0.002	7.58354	17.491	-0.099	-0.089
5	191183	0.159 ± 0.022	0.126 ± 0.023	1.152 ± 0.096	84.8 ± 1.1	0.178 ± 0.003	3.28794	18.212	-0.024	0.012
6	11143*	0.147 ± 0.007	0.093 ± 0.009	1.366 ± 0.093	85.9 ± 0.9	0.161 ± 0.002	5.72586	16.164	-0.129	-0.101
6	67289*	0.157 ± 0.015	0.139 ± 0.014	1.207 ± 0.058	86.6 ± 0.6	0.068 ± 0.002	3.29158	15.939	-0.231	-0.035
6	191016	0.193 ± 0.020	0.134 ± 0.015	1.108 ± 0.132	87.2 ± 3.2	0.156 ± 0.006	1.92518	18.827	-0.018	0.158
6	222388	0.131 ± 0.013	0.077 ± 0.009	1.098 ± 0.147	89.1 ± 5.3	0.014 ± 0.004	6.61099	18.627	0.027	0.162
7	13487*	0.195 ± 0.022	0.181 ± 0.024	1.068 ± 0.052	83.8 ± 0.5	0.021 ± 0.002	5.71080	15.709	-0.036	-0.113
7	83110*	0.165 ± 0.010	0.113 ± 0.018	1.051 ± 0.062	86.2 ± 1.7	0.225 ± 0.002	5.29831	17.238	-0.190	-0.149
8	35399	0.135 ± 0.025	0.095 ± 0.042	1.200 ± 0.184	86.2 ± 3.5	0.315 ± 0.003	4.68531	18.282	-0.050	-0.008
8	39206*	0.196 ± 0.013	0.125 ± 0.012	1.110 ± 0.109	86.8 ± 2.7	0.125 ± 0.004	3.92190	18.042	-0.005	0.074
8	53788*	0.141 ± 0.033	0.126 ± 0.037	1.086 ± 0.065	87.6 ± 1.7	0.041 ± 0.003	5.10280	18.108	-0.090	-0.013
9	55949	0.155 ± 0.009	0.105 ± 0.009	0.946 ± 0.074	88.0 ± 2.2	0.005 ± 0.002	63.98542	17.459	0.834	0.926
9	67706*	(0.156 ± 0.008)	0.106 ± 0.012	0.924 ± 0.078	87.5 ± 2.5	0.004 ± 0.002)				
9	89664*	0.173 ± 0.008	0.119 ± 0.016	1.345 ± 0.088	85.3 ± 1.6	0.163 ± 0.002	3.25213	16.912	-0.157	-0.121
9	89664*	0.139 ± 0.033	0.130 ± 0.036	1.327 ± 0.149	86.8 ± 1.7	0.021 ± 0.003	2.34910	18.088	-0.157	-0.092
10	22190*	0.191 ± 0.020	0.144 ± 0.023	1.358 ± 0.163	83.7 ± 1.6	0.040 ± 0.003	1.44831	18.025	-0.120	-0.049
10	39758*	0.175 ± 0.011	0.138 ± 0.014	1.303 ± 0.148	89.0 ± 4.9	0.019 ± 0.003	3.35275	15.882	-0.229	-0.155
10	68458*	0.160 ± 0.016	0.135 ± 0.017	1.082 ± 0.046	85.6 ± 0.5	0.049 ± 0.002	3.40799	17.284	-0.190	-0.149
10	108195*	0.188 ± 0.016	0.174 ± 0.019	1.278 ± 0.080	81.9 ± 0.5	0.001 ± 0.003	2.26354	17.206	-0.150	-0.110
10	137844†	0.186 ± 0.003	0.147 ± 0.003	1.103 ± 0.038	89.3 ± 1.5	0.008 ± 0.001	248.00000	14.609	1.016	1.121
		(0.192 ± 0.004)	0.148 ± 0.004	1.022 ± 0.029	88.7 ± 1.0	0.008±0.001)				

Table 4: Table of parameters for eclipsing binaries selected as likely distance indicators on the basis of being well detached. The periods, I-magnitudes and colors are taken from Udalski et al. (1998). Those marked with an asterisk appeared in the list compiled by Udalski et al. (1998). The solutions marked with a dagger also appear in Tab. 5. Second solutions for the two red, long period objects assuming different limb-darkening coefficients are given in parentheses.

Field	Object	Radius of star 1 $\frac{R_1}{a}$	Radius of star 2 $\frac{R_2}{a}$	Surf.-bright. ratio $\frac{J_1}{J_2}$	inclination $i$ (degrees)	eccentricity $e$	Period (days)	I	B-V	V-I
3	193413	0.400 ± 0.012	0.192 ± 0.005	1.392 ± 0.087	84.3 ± 1.7	0.011 ± 0.002	0.76458	17.013	-0.001	0.124
4	75638*	0.281 ± 0.012 (0.277 ± 0.012)	0.148 ± 0.007 0.145 ± 0.012	1.022 ± 0.056 1.016 ± 0.060	84.7 ± 1.8 85.2±1.8	0.068 ± 0.003 (0.068 ± 0.003)	2.65340	17.972	0.162	0.780
4	103706*	0.388 ± 0.006	0.179 ± 0.004	1.166 ± 0.035	82.4 ± 0.9	0.006 ± 0.002	1.35588	15.395	-0.211	-0.205
4	175333*	0.253 ± 0.009	0.143 ± 0.007	1.278 ± 0.084	85.0 ± 1.5	0.012 ± 0.003	1.25116	17.653	-0.125	-0.056
5	16658*	0.345 ± 0.007	0.200 ± 0.004	1.174 ± 0.040	85.7 ± 1.3	0.002 ± 0.002	1.24619	17.414	-0.148	-0.100
5	43860	0.422 ± 0.016	0.173 ± 0.009	1.069 ± 0.087	81.9 ± 2.0	0.005 ± 0.005	1.40380	17.745	0.085	0.146
5	129441*†	0.199 ± 0.004	0.128 ± 0.003	1.012 ± 0.026	87.3 ± 0.8	0.375 ± 0.001	8.05053	15.991	-0.128	-0.071
5	196565*	0.204 ± 0.006	0.116 ± 0.003	1.074 ± 0.036	88.7 ± 2.5	0.085 ± 0.002	3.94260	16.910	9.999	9.999
5	266131	0.332 ± 0.008	0.216 ± 0.009	1.363 ± 0.067	85.1 ± 1.5	0.003 ± 0.003	1.30288	17.017	-0.051	-0.014
5	283079*	0.272 ± 0.006	0.233 ± 0.007	1.055 ± 0.027	88.5 ± 1.8	0.001 ± 0.001	1.28358	17.374	-0.074	0.028
5	300727*	0.298 ± 0.009	0.169 ± 0.006	1.465 ± 0.100	87.0 ± 2.6	0.003 ± 0.003	1.57142	17.168	-0.060	0.025
6	77359*	0.228 ± 0.010	0.133 ± 0.007	1.170 ± 0.079	85.5 ± 1.4	0.101 ± 0.003	3.68834	16.472	-0.175	0.074
6	158178	0.207 ± 0.006	0.123 ± 0.004	1.204 ± 0.062	88.1 ± 2.1	0.242 ± 0.002	2.16926	16.538	-0.201	-0.199
6	180306*	0.201 ± 0.004	0.155 ± 0.004	1.374 ± 0.061	88.3 ± 1.0	0.042 ± 0.002	4.59712	17.099	-0.087	-0.042
6	215965	0.391 ± 0.006	0.171 ± 0.004	1.099 ± 0.034	83.0 ± 1.0	0.004 ± 0.002	3.94604	14.116	-0.204	-0.209
6	242137	0.373 ± 0.008	0.179 ± 0.005	1.187 ± 0.049	82.4 ± 1.0	0.008 ± 0.003	2.45717	17.204	9.999	9.999
6	319966	0.392 ± 0.009	0.170 ± 0.006	1.098 ± 0.050	81.1 ± 1.2	0.012 ± 0.003	1.06463	16.282	-0.142	-0.109
7	115361*	0.328 ± 0.008	0.192 ± 0.005	1.192 ± 0.048	87.6 ± 2.8	0.016 ± 0.002	1.57361	17.018	-0.106	-0.086
7	133897*	0.273 ± 0.006	0.190 ± 0.004	1.266 ± 0.040	88.4 ± 2.0	0.028 ± 0.002	1.59029	17.147	-0.162	-0.149
7	255621*	0.215 ± 0.007	0.136 ± 0.005	1.255 ± 0.059	88.9 ± 2.8	0.144 ± 0.002	4.33063	16.180	-0.177	-0.111
7	255917*	0.356 ± 0.012	0.181 ± 0.007	1.067 ± 0.052	82.9 ± 1.4	0.004 ± 0.004	1.52412	17.737	-0.022	0.059
8	42722	0.206 ± 0.008	0.121 ± 0.007	1.066 ± 0.079	86.4 ± 1.5	0.058 ± 0.002	2.69232	17.551	-0.091	-0.037
8	76421	0.316 ± 0.008	0.179 ± 0.010	1.440 ± 0.110	83.5 ± 1.6	0.003 ± 0.003	1.92885	17.703	-0.128	-0.088
8	119647	0.433 ± 0.016	0.182 ± 0.006	1.065 ± 0.059	84.3 ± 2.5	0.004 ± 0.004	0.85494	17.631	-0.092	-0.129
8	163828	0.223 ± 0.013	0.128 ± 0.010	1.107 ± 0.093	85.2 ± 1.8	0.207 ± 0.004	3.93281	17.794	-0.076	0.046
10	114	0.398 ± 0.012	0.164 ± 0.006	1.105 ± 0.072	81.3 ± 1.5	0.001 ± 0.004	1.03348	17.041	-0.138	-0.057
10	6166	0.302 ± 0.007	0.189 ± 0.006	1.202 ± 0.046	84.8 ± 1.1	0.014 ± 0.001	2.57091	17.431	-0.078	-0.029
10	78731*	0.322 ± 0.006	0.189 ± 0.004	1.178 ± 0.037	86.8 ± 1.5	0.013 ± 0.002	1.42945	16.904	-0.196	-0.154
10	137844†	0.186 ± 0.003 (0.192 ± 0.004)	0.147 ± 0.003 0.148 ± 0.004	1.103 ± 0.038 1.022 ± 0.029	89.3 ± 1.5 88.7±1.0	0.008 ± 0.001 0.008±0.001)	248.00000	14.609	1.016	1.121

Table 5: Table of parameters for eclipsing binaries selected as likely distance indicators based on their having complete eclipses. The periods, I-magnitudes and colors are taken from Udalski et al. (1998). Those marked with an asterisk appeared in the list compiled by Udalski et al. (1998). The solutions marked with a dagger also appear in Tab. 4. Second solutions for the red objects 4-75638 and 10-137844 assuming different limb-darkening coefficients are given in parentheses.